nature communications

Article

https://doi.org/10.1038/s41467-026-71281-7

Downregulated transcription in chromosomal domains of midbrain dopamine neurons linked to schizophrenia

Received: 29 October 2024

Accepted: 16 March 2026

Published online: 06 April 2026

Check for updates

Swadha Singh[1,2], Marina Iskhakova[1,2], Tova Y. Lambert[1,2], Aditi Valada[1,2], Neda Shokrian[1,2], Viviana Evans[1,2], Jaroslav Bendl[1,3,4], Pavan K. Auluck[5], Stefano Marenco[5], Minghui Wang[4,6,7], Bin Zhang[4,6,7,8], Gabriel E. Hoffman[1,3,4,9], Kiran Girdhar[1,3,4] ✉, Panos Roussos[1,2,3,4,9,10] ✉ & Schahram Akbarian[1,2,4] ✉

Ventral midbrain dopaminergic neurons are a key cell type for schizophrenia pathophysiology but information about cell type-specific genomic dysregulation in diseased brains is missing. We generated a unique midbrain functional genomics resource with 97 RNA-seq and 34 Hi-C chromosomal contact libraries for Nurr1 + /NeuN+ dopaminergic and their surrounding Nurr1-/NeuN- nuclei, collected from donors diagnosed with schizophrenia (SCZ), bipolar disorder (BD) and compared to neurotypical controls. Among the 954 dopamine neuron genes specifically dysregulated in SCZ, 331 were downregulated, with selective enrichment for risk-associated synaptic plasticity and neuronal connectivity pathways and embedded within dopamine neuron-specific topologically associated chromosomal domains (TAD). Transcript-resolved analysis revealed 2,350 transcripts with altered expression in SCZ dopamine neurons, affecting key susceptibility genes such as the *FOXP1, MAPK10, PCM1 and NRXN1*. Therefore, genomic dysregulation in the ventral midbrain of subjects diagnosed with SCZ selectively affects dopaminergic neurons, and includes a unilateral association of genetic risk with down-, but not upregulated transcription at the sites of highly organized chromosomal domains harboring neuron-specific genes with complex transcriptional architectures.

Schizophrenia (SCZ) and bipolar disorder (BD) are major psychiatric disorders, each affecting approximately 1% of the population worldwide. No unifying neuropathology exists, but there is a complex genetic risk architecture that includes, for SCZ, non-coding variants within 287 distinct loci, each contributing a very small but tractable liability[1], together with a few dozen very rare mutations and variants of much higher disease penetrance[2]. Therefore, exploration of genome organization and function in the brains of subjects diagnosed with SCZ

[1]Department of Psychiatry, Icahn School of Medicine at Mount Sinai, New York, NY, USA. [2]Friedman Brain Institute, Icahn School of Medicine at Mount Sinai, New York, NY, USA. [3]Center for Disease Neurogenomics, Icahn School of Medicine at Mount Sinai, New York, NY, USA. [4]Department of Genetics and Genomic Sciences, Icahn School of Medicine at Mount Sinai, New York, NY, USA. [5]Human Brain Collection Core, National Institute of Mental Health–Intramural Research Program, Bethesda, MD, USA. [6]Mount Sinai Center for Transformative Disease Modeling, Icahn School of Medicine at Mount Sinai, New York, NY, USA. [7]Icahn Genomics Institute, Icahn School of Medicine at Mount Sinai, New York, NY, USA. [8]Department of Pharmacological Sciences, Icahn School of Medicine at Mount Sinai, New York, NY, USA. [9]Mental Illness Research Education and Clinical Center (MIRECC), James J. Peters VA Medical Center, Bronx, NY, USA. [10]Center for Precision Medicine and Translational Therapeutics, James J. Peters VA Medical Center, Bronx, NY, USA. ✉e-mail: kiran.girdhar@mssm.edu; panagiotis.roussos@mssm.edu; schahram.akbarian@mssm.edu

and BD, and comparison with neurotypical brains, carries significant potential to uncover disease-sensitive transcriptomic and epigenomic alterations. To date, however, at base pair resolution, very few genome-scale case-control brain reference sets for gene expression, DNA methylation, chromatin accessibility, and histone marks exist, and moreover, these are exclusively limited to the frontal lobe, including its higher association cortex[3–7] and portions of the rostral striatum[8,9], and the medial temporal lobe, including the hippocampus[10,11].

Unfortunately, to date, there are no genomic studies on critical nodes of the psychosis circuitry outside of the aforementioned frontal and temporal lobe areas, despite the numerous times they have been implicated. For example, functional neuroimaging studies identified the dysregulation of dopaminergic neurons in the ventral midbrain as the critical presynaptic component responsible for altered dopaminergic innervation and signaling in SCZ and BD forebrain[12]. Moreover, a pilot study on brain tissue homogenate from 28 diseased brains, measuring expression levels of 12 markers commonly associated with presynaptic dopaminergic signaling, reported alterations in a small subset of subjects[13]. However, perhaps the most compelling rationale for studying dopaminergic systems in schizophrenia and related diseases is provided by the undisputed fact that to date, antipsychotic drugs (e.g., haloperidol, aripiprazole, and cariprazine) targeting D_2 and other dopamine receptor systems are still the mainstay of treatment worldwide[14]

This lack of genomic reference sets from SCZ and BD midbrain could be a reflection of technical challenges presented by the very minor share of dopaminergic neurons in brain tissue. Indeed, even in some of the most compact anatomical structures harboring dopaminergic neurons such as the substantia nigra (SN) and bordering ventral tegmental area (VTA), also known as dopaminergic cell clusters A9 and A10, respectively, less than 2% of the total cell population express presynaptic dopaminergic marker genes[15–17] and thereby are likely to evade functional genomic profiling if bulk tissue without cell-targeted enrichment would serve as the input material.

Here, we bypass these limitations by applying immunotagging combined with fluorescence-activated nuclei sorting (FANS) of ventral midbrain tissue to separately collect dopaminergic neuron nuclei and their surrounding non-neuronal nuclei, followed by deep cell-type specific profiling of the nuclear transcriptome (nucRNA-seq) together with "HiC" 3D genome chromosomal conformation mapping to differentiate between active and inactive chromosomal compartments and domains. Our functional genomics resource encompasses 97 subject and cell-type-specific nuclear transcriptomes and 34 subject and cell-type-specific 3D genomes. Each dataset is deeply sequenced, with average read counts of 59 and 649 million reads per RNA-seq and Hi-C library, respectively. We thereby provide reference maps for the ventral midbrain of a SCZ and BD cohort compared to neurotypical controls and report disease-specific alterations in dopamine neuron-specific gene expression in the context of the underlying genetic risk architecture and 3D genome organization.

Results

Dopaminergic neurons in the midbrain are enriched with SCZ risk genes

To understand the role of dopaminergic neurons in SCZ in the midbrain region, we utilized a postmortem brain cohort comprised of 73 donors (1) from the CommonMind Consortium collection[18]. As illustrated in Fig. 1A, we first profiled a total of 97 RNA-seq libraries by immunotagging nuclei extracts from ventral midbrain SN (area A9) for previously validated[1] FANS sorting of dually labeled nuclei that were NeuN+ (pan-neuronal marker) and Nurr1+ (nuclear receptor subfamily 4 group A member 2 (NR4A2), a transcription factor crucial for maintenance and development of dopaminergic neuron)[19,20] (Fig. S1A). From the same tissues, we sorted and collected the surrounding non-neuronal (predominantly glial) Nurr1-/NeuN- nuclei (Fig. S1B). Altogether, we generated 41 Nurr1+/NeuN+ dopamine neuron-specific ("dopa neurons") RNA-seq libraries, comprising 24 control, 8 SCZ, and 9 BD ventral midbrain samples. Additionally, 56 Nurr1-/NeuN- non-neuron specific ("non-neurons") were collected from 26 controls, 22 SCZ, and 8 BD midbrains. The samples were sequenced to an average depth of 59 ± 5.3 million reads (Fig. S2).

All processed data went through a series of rigorous quality control steps, as shown in Fig. S2 and explained in detail in "Methods" (Supplementary Data 1). Metadata for all QC-passed samples, including sex, ancestry, age, postmortem interval, and RIN, stratified by cell type and diagnosis, are shown in Fig. S3C, illustrating demographic and quality metrics across groups. To assess overall transcriptomic structure, we performed principal component analysis (PCA) on $\log_2$CPM-normalized expression, which clearly separated dopaminergic and non-neuronal samples (Fig. 1B). We next validated the cell-type specificity of the sorted populations through deconvolution[21] against a published single-cell ventral midbrain reference[22]. This analysis confirmed that FANS-sorted dopaminergic nuclei were highly enriched for dopaminergic signatures (~80.9% ± 0.0206), while non-neuronal nuclei were enriched for non-neuronal signatures (~97.9% ± 0.00320) (Figs. 1C and S2E).

Our initial analysis focused on exploring the statistical differences in the transcriptomes of Nurr1+NeuN+ dopa neurons and Nurr1-NeuN- non-neurons in controls. As expected, the majority (~25%) of variation in transcriptome expression came from cell types (dopa and non-neurons) (Fig. S2B). Furthermore, more than two-thirds of the transcriptome (20,549 out of 30,687, 67%) showed significant changes at FDR < 0.05, including $N = 10{,}383$ genes (33.84%) in dopa neurons and $N = 10{,}166$ (33.13%) in non-neurons (Fig. 1D and Supplementary Data 2A). Inspection of known cell type marker genes further confirmed the specificity of our sorted populations. For example, dopaminergic neuron samples exhibited strong expression of *Tyrosine Hydroxylase (TH)* (logFC = 2.8; FDR = 7.7×10^{-7}), the rate-limiting enzyme in dopamine synthesis, while non-neuronal samples showed robust expression of *Olig2* (logFC = −5.04; FDR = 3.8×10^{-19}), a transcription factor specific to oligodendrocytes, which constitute the majority (>65%) of cells in the SN[15] (Fig. 1E).

Notably, dopa-specific transcriptomes showed strong enrichments for psychiatric and neurological disease risk genes, including SCZ, BD, MDD (major depressive disorder), and PD (Parkinson's disease), using MAGMA[23] ("Method" and Supplementary Data 2B). In contrast, the non-neuron-specific transcriptome showed enrichment for various immunological and other non-brain-related traits such as height (Fig. 1F). Functional pathway analysis of the dopa-specific transcriptome was predominantly associated with neuron-specific pathways like synaptic signaling, sharply contrasting with the non-neuron-specific transcriptome, which was primarily enriched for immune response and cytokine production pathways (Fig. S2D and Supplementary Data 2C). Together, these results establish that our sorted populations capture highly cell–type–specific transcriptomic programs, providing a robust framework to investigate the role of dopaminergic neurons in SCZ.

Downregulated dopa neuronal transcriptome in SCZ is associated with brain-related traits

We next assessed disease-related transcriptional changes in 8 SCZ and 9 BD donors compared to 24 controls for dopa neuronal samples, and in 22 SCZ and 8 BD donors compared to 26 controls for non-neuronal samples. To account for biological and technical variability, we modeled variance contributions in gene expression across covariates (Figs. 2A and S3A) and included cell-type proportion estimates, i.e., dopa neuron proportion in dopa neuronal samples and non-neuronal proportion (oligodendrocytes) in non-neuronal samples (Fig. 1C) as covariates. This approach ensured that disease-associated changes

https://doi.org/10.1038/s41467-026-71281-7

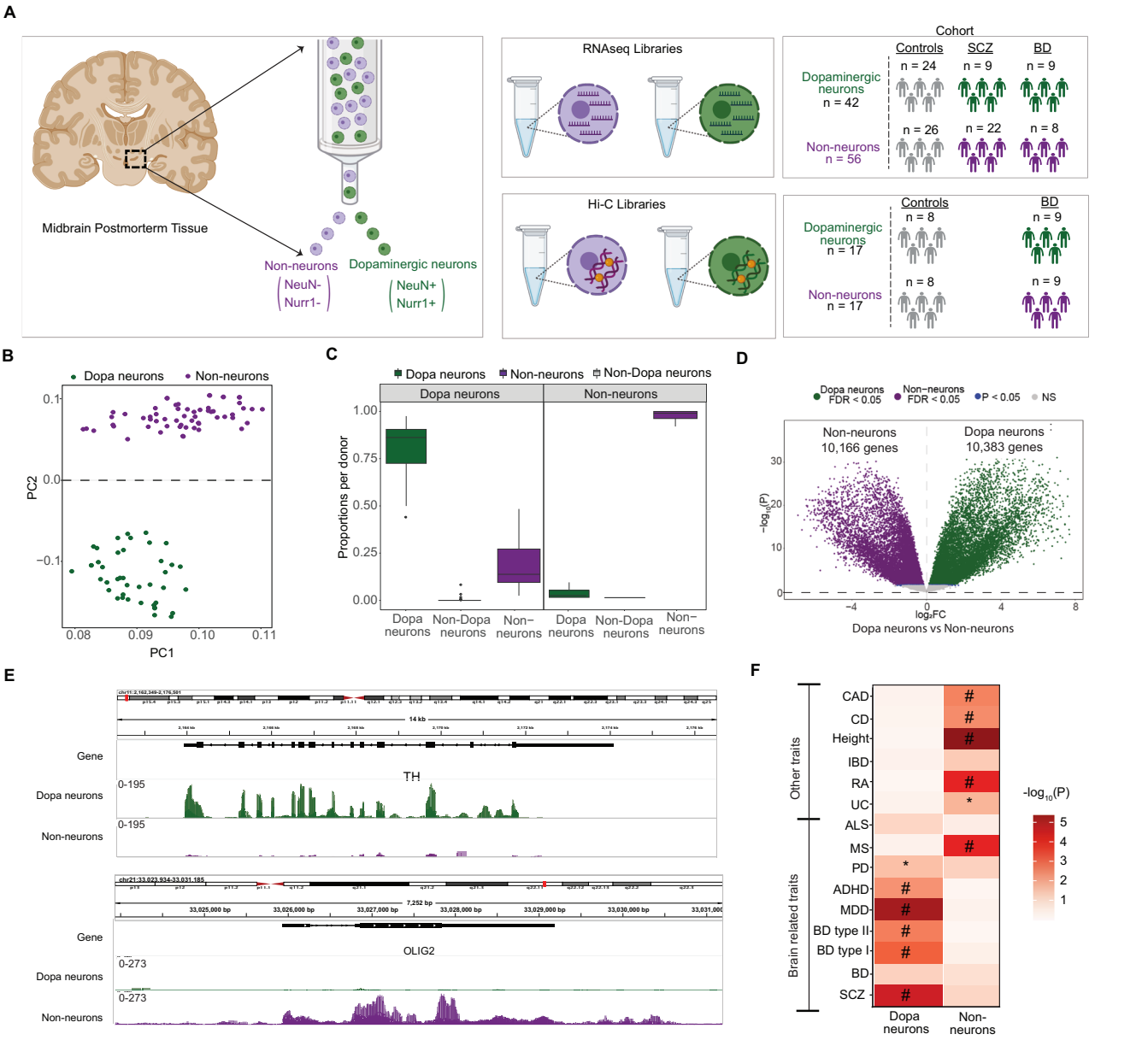

Fig. 1 | Cell type-specific transcriptome in the midbrain. A The schematic (Created in BioRender. Singh, S. (2025) https://BioRender.com/cds9815) shows FANS of our two populations, with dopaminergic neuron nuclei (Nurr1+/NeuN+, green) and surrounding non-neuronal nuclei (Nurr1−/NeuN−, purple) isolated from post-mortem midbrain tissue. From these sorted nuclei, we generated 97 RNA-seq libraries and 34 Hi-C libraries to profile the transcriptome and 3D genome organization, respectively. **B** PCA of log_2CPM expression values from 97 RNA-seq samples. **C** Boxplot displaying the cumulative proportion of dopa and non-neuronal samples derived using the reference[22] basis sets from single-cell midbrain data collapsed into three categories: (1) dopa ($n = 50$), (2) non-dopa neurons ($n = 22$) and (3) non-neurons ($n = 100$). Box plots display the median (center line), the 25th and 75th percentiles (bounds of the box), and whiskers extending to the minimum and maximum values within 1.5× the interquartile range. Individual points represent biological replicates (independent samples). No statistics were derived from technical replicates. **D** Volcano plot of −log10(P) vs. log2FC for differential expression between dopa neurons ($n = 24$) and non-neuronal samples ($n = 26$). Differential expression was tested using a dream linear mixed-effects model with limma empirical-Bayes moderation, yielding two-sided moderated t-tests. *P* values are shown with Benjamini–Hochberg FDR correction. Genes significantly up- and down-regulated at FDR < 0.05 are shown in green and purple, respectively. **E** An example of $n = 5$ libraries to demonstrate genomic coverage of dopa neuronal specific (TH) and non-neuronal specific (olig2) genes. **F** MAGMA gene-set enrichment analysis of dopa-neuronal (10,383) and non-neuronal (10,166) specific genes across brain-related, neurodegenerative, and non-brain traits. Enrichment coefficients (BETA) and *P* values were obtained from the MAGMA multiple-regression model using a two-sided test of the regression coefficient (Z-test). Exact *P* values are displayed as −log10(P). Multiple-testing correction was performed using the Benjamini-Hochberg FDR. "#" indicates FDR < 0.05; "*" indicates nominal significance at $P < 0.05$. Trait abbreviations: ADHD Attention-Deficit/Hyperactivity Disorder, ALS Amyotrophic Lateral Sclerosis, BD Bipolar Disorder, BD I Bipolar Disorder type I, BD II Bipolar Disorder type II, CAD Coronary Artery Disease, CD Crohn's Disease, Height Height, IBD Inflammatory Bowel Disease, MDD Major Depressive Disorder, MS Multiple Sclerosis, PD Parkinson Disease, RA Rheumatoid Arthritis, SCZ Schizophrenia, UC Ulcerative Colitis.

reflect true gene dysregulation rather than differences in cellular composition across donors.

Using this model, we identified 954 differentially expressed genes (623 up, 331 down; FDR < 0.05) in SCZ dopa neurons (Fig. 2B and Supplementary Data 3A). No FDR-significant changes were observed in the non-neuronal samples despite the higher statistical power to detect differences in SCZ (Fig. S5A and Supplementary Data 3B). Functional enrichment revealed that downregulated genes in SCZ

https://doi.org/10.1038/s41467-026-71281-7

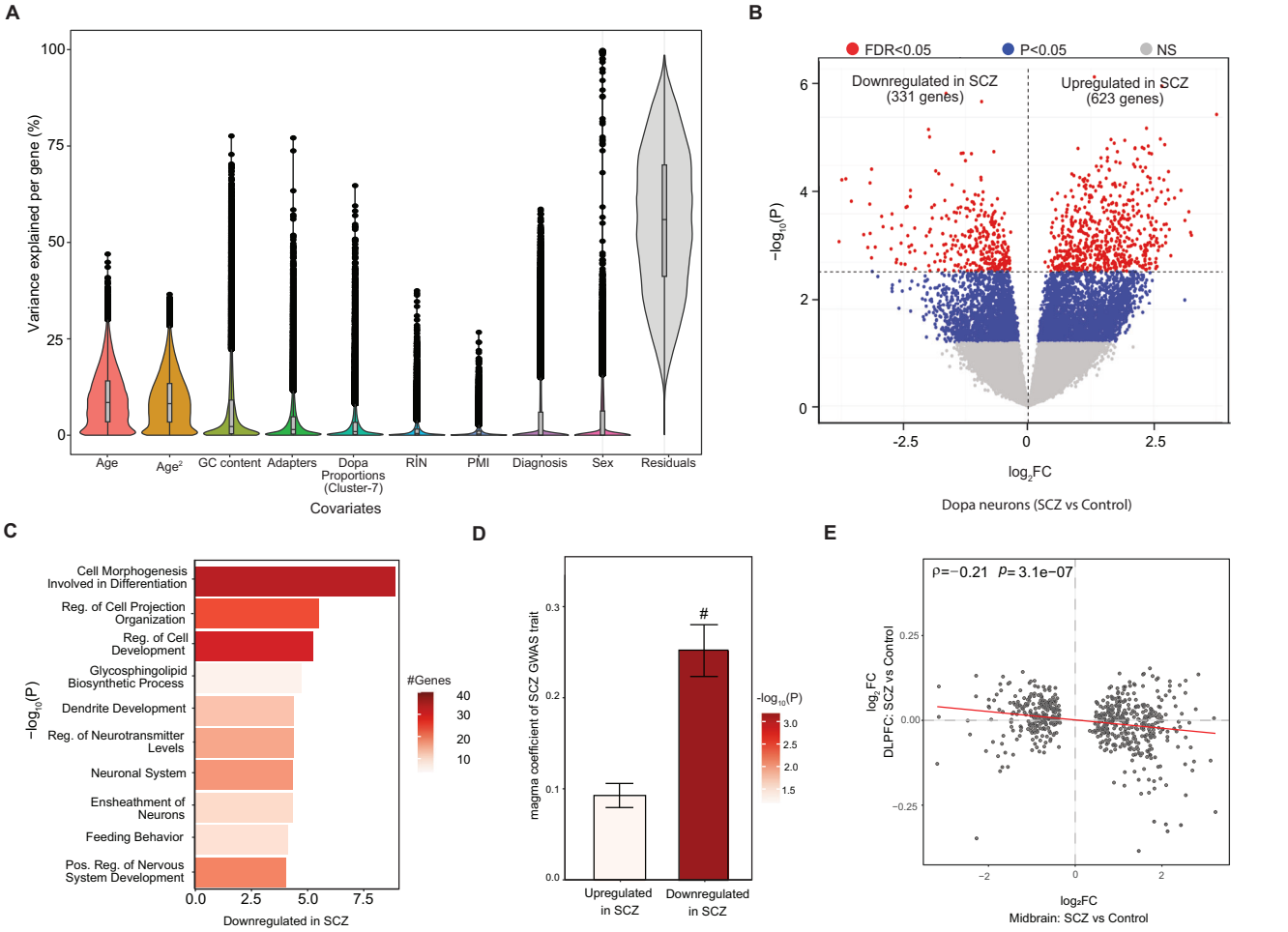

Fig. 2 | SCZ-specific transcriptome in dopa neurons. A Violin plots to show the distribution of variance for biological and technical covariates in the gene expression of dopa neurons in 41 (24 Control, 8 SCZ, 9 BD) samples. RIN: RNA integrity number. Box plots are depicted with the center line indicating the median, the box representing the interquartile range (between the 25th and 75th percentiles), and whiskers extending to the lowest and highest values within 1.5 times the interquartile range from the median. Dots are used to indicate potential outliers beyond this range. **B** Volcano plot of −log10(P) vs. log2FC for differential gene expression between SCZ ($n = 8$) and control ($n = 24$) dopa-neuron samples. Differential expression was tested using the dream linear mixed-effects model with limma empirical-Bayes moderation, yielding two-sided moderated t-tests with Benjamini–Hochberg FDR correction. Genes in blue are nominally significant at $P < 0.05$, and genes in red are significant at FDR < 0.05. **C** Bar plot showing GO pathway enrichment for genes downregulated in SCZ. Enrichment P values were obtained from the MAGMA gene-set regression model using a two-sided test of the regression coefficient, and are displayed as −log10(P). Multiple-testing correction was performed using the Benjamini–Hochberg FDR. Bar color indicates the number of genes overlapping each pathway. **D** MAGMA gene set enrichment analysis of upregulated ($n = 623$) and downregulated ($n = 331$) genes in SCZ for enrichment in SCZ genetic risk. We applied multiple testing across all 2 datasets, which are shown as x-axis in the plot. FDR values correspond to false discovery rate (adjusted q values); bars marked "FDR < 0.05" meet the significance threshold. Bars represent mean values, and error bars indicate ±standard error of the mean (SEM) of SCZ heritability coefficients from MAGMA analysis. **E** Spearman correlation of $\log_2$FC(SCZ vs. Controls) between midbrain (at FDR < 0.05 on X-axis) and dorsolateral prefrontal cortex, DLPFC (Y-axis).

dopaminergic neurons were enriched for pathways related to neuronal connectivity and signaling, including *r*egulation of neurotransmitter levels, neuronal system, ensheathment of neurons, and positive regulation of nervous system development (Fig. 2C). By contrast, upregulated genes mapped largely to structural and organizational pathways, including one neuro-related pathway, synaptic signaling (Fig. S3B and Supplementary Data 3C).

MAGMA analysis confirmed that downregulated genes, but not upregulated genes, were significantly enriched for SCZ genetic risk (Fig. 2D and Supplementary Data 3D). Among the top disease-associated downregulated genes were *SLC6A3* (dopamine transporter, DAT) and *SLC18A2* (vesicular monoamine transporter, VMAT2), key regulators of dopamine reuptake and storage (Fig. S4A). Their repression is consistent with long-standing evidence of dopaminergic dysfunction in SCZ, including the dopamine hypothesis and prior postmortem findings[24,25]. In addition, top upregulated genes in dopaminergic neurons from SCZ donors include MTND1P23, CTD-2336H13.1, and RP11-149A16.12 (Fig. S4A). While their precise roles in neuronal function are less well characterized compared to DAT and VMAT2, their consistent upregulation highlights disease-associated transcriptional shifts that may reflect compensatory processes, mitochondrial activity, or structural reorganization in SCZ neurons. Together, these findings emphasize that SCZ pathophysiology involves both suppression of key dopaminergic regulators and activation of other molecular programs, reinforcing the complexity of transcriptional dysregulation in the disorder.

To evaluate potential medication effects, we compared antipsychotic-exposed and unexposed donors within SCZ (1 unexposed, 8 exposed) and BD groups (7 unexposed, 2 exposed), separately for neuronal and non-neuronal samples. Across all comparisons, no significant genes were detected at FDR < 0.05 (Fig. S4B–E and Table S3E–H). These findings are consistent with prior reports suggesting that antipsychotic treatment may have only a limited impact

on postmortem transcriptional profiles[26,27]; however, this cannot be stated with certainty given the limited sample size.

For BD donors, no differentially expressed genes were detected relative to controls in either neuronal or non-neuronal fractions (FDR < 0.05; Fig. S5A and Table S3I, J). Nevertheless, comparison of disease signatures revealed a negative concordance between SCZ and BD in dopaminergic neurons ($\rho = -0.34$, $p < 2.2 \times 10^{-16}$) and a positive concordance in non-neurons ($\rho = 0.087$, $p < 2.2 \times 10^{-16}$) (Fig. S5B, C).

To assess subtype specificity, we leveraged single-cell reference data from Wang et al[22]. and tested cluster-level enrichment of SCZ-associated genes. Downregulated genes were most enriched in the C7 dopaminergic subtype (TH/SLC6A3/ALDH1A1-positive), followed by the C6 dopaminergic subtype (TH/SLC6A3-positive) and the C9 GABAergic subtype (Fig. S7A), indicating a selective repression of dopaminergic programs in SCZ. Of note, modest enrichment was also observed in the non-neuronal C0 cluster, although this signal was weaker and less specific than that in dopaminergic subtypes.

Finally, we compared midbrain findings with published SCZ-associated genes from homogenate dorsolateral prefrontal cortex (DLPFC) and anterior cingulate cortex (ACC) in the CommonMind Consortium dataset[18]. In contrast to midbrain dopa neurons, DLPFC and ACC homogenates showed enrichment of upregulated but not downregulated genes for SCZ risk (Fig. S6A–C and Supplementary Data 3K). Correspondingly, SCZ vs. control and BD vs. control gene expression changes in DLPFC and ACC were positively correlated (DLPFC $\rho = 0.57$; ACC $\rho = 0.52$; both $p < 2.2 \times 10^{-16}$), in sharp contrast to the negative concordance observed in midbrain dopa neurons ($\rho = -0.34$, $p < 2.2 \times 10^{-16}$; Fig. S6D–F). Consistent with this regional divergence, comparison of schizophrenia-associated differential expression between midbrain and DLPFC revealed a modest but significant negative correlation ($\rho = -0.21$, $p = 3.1e{-}07$), indicating regionally opposing transcriptional changes (Fig. 2E). Together, these results reveal a region- and cell-type-specific pattern of dysregulation: midbrain dopa neurons in SCZ exhibit broad gene expression repression of neuronal genes tied to genetic risk, whereas cortical regions show the opposite trend, with risk associated primarily with upregulated expression.

SCZ-associated genes exhibit concordant or discordant transcript-level effect sizes

Alternative splicing and variation in transcription start/stop sites have been implicated in SCZ pathogenesis[26,28]. Because gene-level analyses may mask such isoform-specific effects, we examined transcript-level regulation in midbrain sorted populations: dopa neurons and non-neurons. We first tested 90,479 transcripts from 38,656 genes using limma, but given the burden of multiple testing corrections, this yielded only 8 significant transcripts in dopa neurons from SCZ versus controls (FDR < 0.05), while no significant differences were observed in BD versus controls or in non-neuronal populations ("Method", Supplementary Data 4A–D).

Given this result, we implemented the random multivariate meta-analysis method, remaCorr[29,30], to examine the relationship between disease-associated changes in Tx expression. remaCorr integrates the estimated SCZ-specific effect sizes of each transcript isoform as a fixed effect, incorporating the inter-correlation matrix between these effect sizes[31]. We further categorized remaCorr-significant genes into *concordant* and *discordant* based on whether their Tx showed uniform or opposing effect sizes ("Methods"). This framework clarifies Tx regulatory interpretation, as discordant genes often reflect more complex isoform-specific mechanisms that may be obscured in gene-level analyses[32–34] (Fig. 3A).

In SCZ dopa neurons, remaCorr identified 294 significant genes comprising 2350 Tx (FDR < 0.05) (Fig. S8B and Supplementary Data 5A), including 164 concordant (73 concordant downregulated and 91 concordant upregulated) and 130 discordant cases (Fig. 3B). Only ~34% overlapped with limma-based results, reflecting that standard gene-level analysis captures concordant genes well but largely misses discordant ones, whose opposing isoform changes cancel at the aggregate level. Consistent with this, concordant genes showed strong π1 (pi-one) enrichment (~0.9), whereas discordant genes displayed weaker enrichment (~0.65). π1 is a statistical estimate of the proportion of true positives among the tested associations, with higher values indicating stronger and more reproducible signals. Discordant genes were also structurally more complex, with a higher number of transcripts (median: 18 ± 9.5 vs. 5 ± 2.9 transcripts) and longer gene bodies (median: 113,352 ± 274,736 vs. 28,750 ± 102,257 bp) compared to concordant genes (Fig. S8C, D). Also, discordant genes exhibited higher variation in disease-associated changes, as reflected by greater standard deviation of $\log_2$ fold-change (Fig. S9A).

Although functional enrichment analyses did not identify neuro-related pathways (Fig. S9C and Supplementary Data 5B), both concordant downregulated and discordant sets were significantly associated with SCZ risk in MAGMA (Fig. 3D and Supplementary Data 5C). For example, *WWOX*, a neurodevelopmental gene linked to epilepsy and neurodegeneration[35], showed discordant transcript regulation (Fig. 3E). Finally, LDSC revealed that discordant downregulated genes were most strongly enriched for SCZ heritability (Fig. S9B).

In BD dopa neurons, remaCorr identified 186 significant genes comprising 1715 Tx (FDR < 0.05) (Fig. S10A), including 89 concordant (51 concordant up and 38 concordant downregulated) and 97 discordant cases (Supplementary Data 5D). Discordant genes, again, were structurally more complex, with a higher number of transcripts (11 ± 9.13 vs. 3 ± 4.42 transcripts) and longer gene bodies (median: 117,819 ± 401,078 bp vs. ~27,700 ± ~195,000 bp) compared to concordant genes. Furthermore, both concordant and discordant Tx genes did not show enrichment for BD risk variants for FDR < 0.05 (Fig. S10B and Supplementary Data 5E). Lastly, in the non-neuronal fraction, neither SCZ nor BD comparisons yielded significant genes at FDR < 0.05 (Fig. S10C, D and Supplementary Data 5F, G).

Together, these results demonstrate that isoform-level dysregulation, especially discordant downregulation, represents an important axis of genetic risk in SCZ, revealing regulatory complexity not captured by gene-level analysis.

3D genome structures associated with altered gene expression in SCZ dopa neurons

Non-randomly occurring "3D" chromosomal conformations play an important role in genome organization and function. Examples include the kilo-to megabase spanning "A" and "B" chromosomal compartments associated with chromatin more permissive ("A") or restrictive ("B") transcriptional environment, in addition to "self-folded" topologically associated domains (TADs) and chromosomal loop formations. Previous work conducted in the DLPFC of SCZ and BD samples has resolved some of these 3D genome elements at chromosomal sites subject to epigenomic and transcriptional dysregulation[6]. To investigate whether SCZ-associated gene dysregulation in midbrain dopa neurons is influenced by 3D genome architecture, we generated 34 deeply sequenced Hi-C libraries from sorted nuclei (17 dopa, 17 non-neuronal; Fig. 1A and Supplementary Data 6). Each set yielded >1.5 billion cis contacts, enabling high-resolution 3D genome maps of the ventral midbrain (Fig. S11C). Clustering of Hi-C profiles using HiCRep[36] separated dopa and non-neuronal samples (Fig. S11D, E), confirming cell type-specific chromosomal conformations consistent with their distinct transcriptomes (Fig. 1D).

We next defined topologically associated domains (TADs) per fraction ($N = 5966$ dopa and $N = 6348$ non-neuronal TADs) using TOPDOM[37]. TAD boundaries in dopaminergic neurons (Fig. S12A–D) were strongly enriched for CTCF[6] (3.283 fold enrichment, $P = 1.19e{-}34$) and the active promoter mark H3K4me3 (2.56 fold enrichment, $P < 1e{-}4$), indicating structural insulation at sites of transcriptional

https://doi.org/10.1038/s41467-026-71281-7

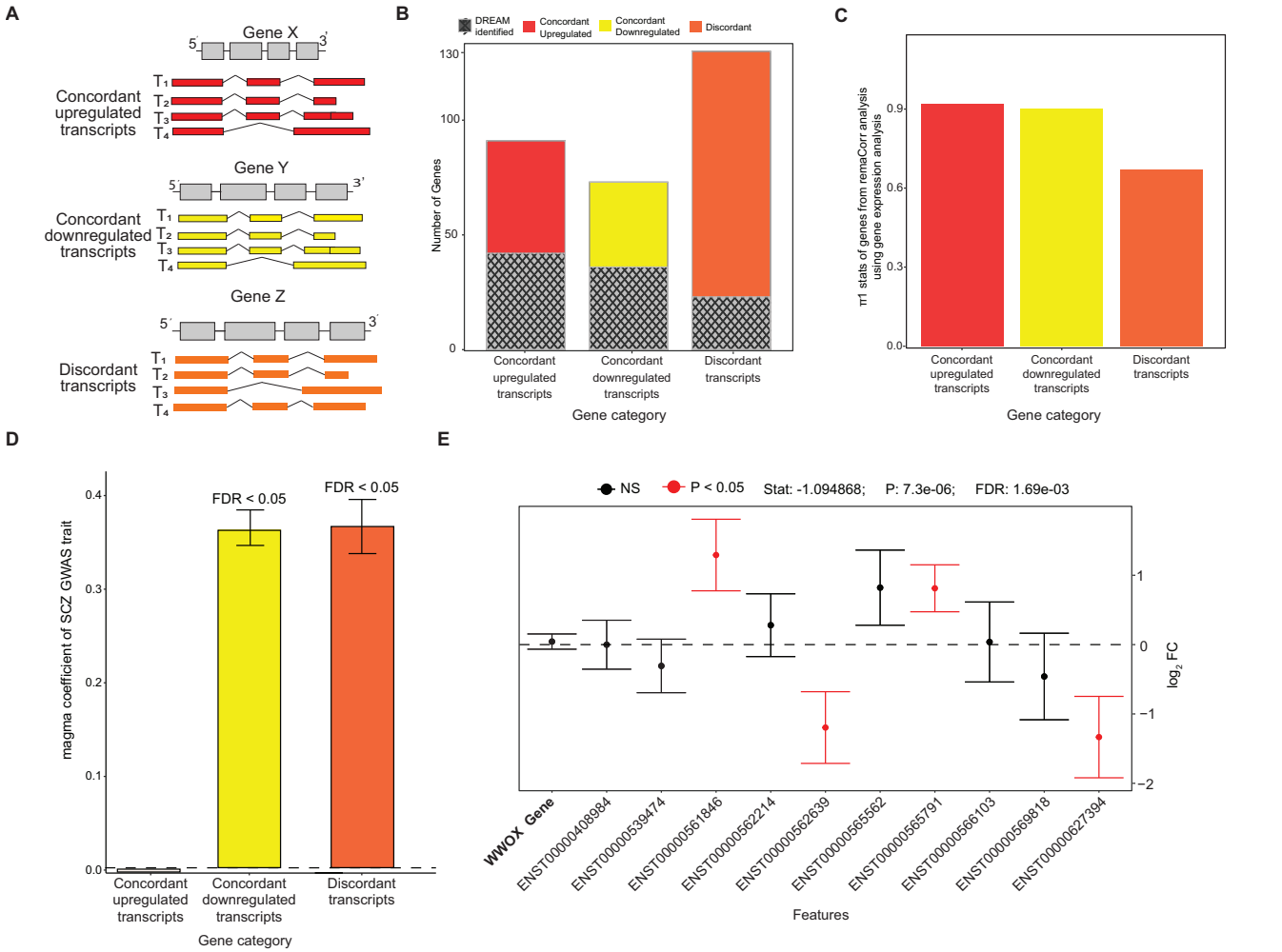

Fig. 3 | SCZ-specific concordant and discordant transcripts in dopa neurons. **A** Genes X and Y are examples of genes with *concordant* transcripts, meaning their transcripts are consistently either upregulated or downregulated, as indicated by the colors red and yellow. In contrast, Gene Z is a *discordant* gene, with its transcripts in orange showing both positive and negative effect sizes. **B** Barplot showing the number of genes that have concordant (up and down) and discordant transcripts. The crosshatch in each bar represents the number of DEG identified in gene analysis (**C**) pi1 stats of genes from remaCorr analysis using gene expression analysis. **D** MAGMA gene set enrichment analysis of concordant (73 downregulated and 91 upregulated) and discordant (130 genes) genes in SCZ for enrichment in SCZ genetic risk. We applied multiple testing across all 3 datasets which are shown as *x*-axis the plot. FDR values correspond to false discovery rate (adjusted *q* values); bars marked "FDR < 0.05" meet the significance threshold. Bars represent mean regression coefficients, and error bars indicate ± SEM. **E** Example of significant discordant genes (WWOX) from remaCorr analysis. Summary statistics of a gene from the remaCorr model, including *P* Values, remaCorr statistics, and FDR values, are added above the plot. The *X*-axis shows the gene and mapped transcripts that are expressed within the gene. The *Y*-axis shows the SCZ-specific effect sizes from limma-based analyses. Effect sizes of transcripts marked in red have limma-based $P < 0.05$, and non-significant transcripts are shown in black. Bars represent the mean effect size for one gene, and error bars show ± SEM.

activity. Similarly, boundaries showed high enrichment for the enhancer-associated histone mark H3K27ac (2.91 fold enrichment, $P = 1.19e{-}34$), while exhibiting marked depletion of the repressive histone mark H3K27me3 (1.964 fold enrichment, $P = 1.14e{-}34$)[38]. Consistent patterns were observed in non-neuronal cells (Fig. S12E–H), where TAD boundaries were enriched for CTCF (2.772 fold enrichment, $P = 1.19e{-}34$) and H3K4me3 (2.765 enrichment, $P = 1.19e{-}34$), as well as H3K27ac (1524 fold enrichment, $P < 1e{-}4$). Like in dopaminergic neurons, boundaries were significantly depleted for H3K27me3 (2.485 fold enrichment, $P = 1.15e{-}34$)[38]. These findings indicate that TAD boundaries in both cell types are flanked by transcriptionally active and structurally defined chromatin, consistent with their role as organizing units of the 3D genome. The high concordance of boundary-associated chromatin marks across dopaminergic and non-neuronal cells supports a conserved architectural framework, despite broader transcriptomic and chromatin state differences between these populations. Similarly, eigenvector analysis identified a total of 39,023 compartments in dopa and 38,991 compartments in non-neurons, using Cscoretools[39] (Supplementary Data 7A), revealing extensive cell type-specific switching between active (A) and inactive (B) chromatin states (Fig. S14B), indicating that risk variants are concentrated within transcriptionally active, regulatory-rich chromatin domains. Specifically, 10,844 bins (27.8%) transitioned from A to B (active in dopa, inactive in non-neurons) and 6545 bins (16.8%) transitioned from B to A (inactive in dopa, active in non-neurons), while the remainder remained stable as either active or inactive in both cell types (A → A or B → B) (Supplementary Data 7B). Furthermore, genes located in stably active A compartments shared between both cell types (A → A) showed a significant positive association with SCZ (Fig. S14C). Genes that gained activity in non-neuronal cells (B → A) exhibited nominal enrichment ($P < 0.05$) for SCZ, suggesting that these regions may represent dynamic chromatin domains that become active during neurodevelopmental transitions. In contrast, genes located in consistently inactive (B → B) or deactivated (A → B) compartments showed

https://doi.org/10.1038/s41467-026-71281-7

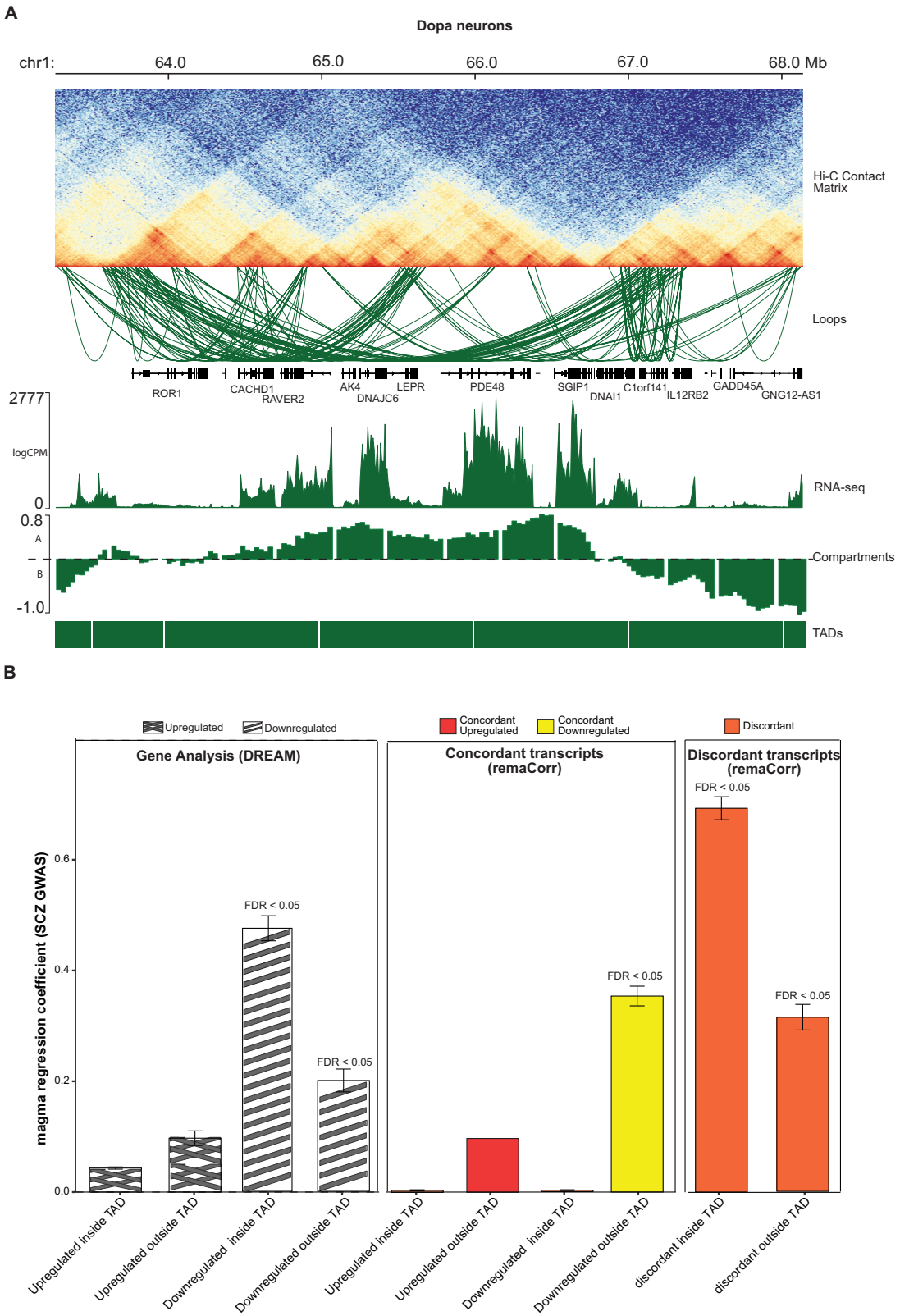

no enrichment, suggesting that SCZ risk is primarily associated with loci in or transitioning toward active chromatin environments.

Figure 4A shows a representative dopaminergic Hi-C contact matrix at a chromosome 1 locus spanning 12 genes, organized into A/B compartments, TADs, and loops at 50 kb resolution. We then examined the spatial organization of SCZ-sensitive genes (from limma and remaCorr; Tables S3A and S5A) within the 3D genome to assess whether they preferentially reside within TADs. We then asked whether SCZ-associated genes identified from gene- and transcript-level analyses (Tables S3A and S5A) preferentially localize to specific 3D features. Downregulated genes within TADs showed the strongest enrichment for SCZ GWAS risk compared to upregulated genes or downregulated genes outside TADs (Fig. 4B and Tables S7B, S7D). For genes with concordant Tx, only genes with downregulated Tx outside

Fig. 4 | The three-dimensional genome of dopa neurons. A The plot of Dopa-neurons showing interaction in a region with HiC contact matrix on the top followed by loops, RNAseq, compartments, and TADs. **B** Bar plots show regression coefficients from MAGMA analysis across three categories: (left panel) gene-level analysis using DREAM (middle panel) concordant transcripts identified by remaCorr, and (right) genes with discordant transcripts identified by remaCorr. DREAM Input genes: Upregulated inside TAD: 60 genes; Upregulated outside TAD: 563 genes; Downregulated inside TAD: 50 genes; Downregulated outside TAD: 281 genes; Concordant transcript input genes: concordant Up inside TAD: 10 genes; concordant up outside TAD: 81 genes; concordant Down inside TAD: 5 genes; concordant Down outside TAD: 68 genes; Discordant transcript input genes: discordant inside TAD: 21 genes; discordant outside TAD: 109 genes); Genes and transcripts are further stratified by expression direction (upregulated or downregulated) and location relative to TADs (inside or outside). We applied multiple testing across all 10 datasets, which are shown as *x*-axis in the plot. FDR values correspond to false discovery rate (adjusted *q* values); bars marked "FDR < 0.05" meet the significance threshold. Bars represent mean regression coefficients, and error bars denote ±SEM.

TADs were enriched (Fig. 4B and Tables S7B, S7E). By contrast, genes with discordant Tx showed robust enrichment both inside and outside TADs, with the strongest effect inside TADs (Fig. 4B and Supplementary Data 7C).

To better understand the structural complexity of dysregulated genes, we next assessed the extent to which dysregulated SCZ dopa neuron genes spanned multiple TADs. A gene was considered to extend across multiple TADs if its full annotated genomic span (from the outermost TSS to the TES across all isoforms) overlapped more than one TAD, while the TSS remained anchored within a single domain. A significantly larger fraction of genes with discordant Tx (34/130) crossed multiple TADs compared to genes with concordant upregulated (10/73) or downregulated (9/91) Tx (Fig. S14A and Supplementary Data 7E, F). These discordant, multi-TAD genes included large, highly spliced, SCZ-implicated loci such as *NRXN1*[40,41], *FOXP1*[42], *MAPK10*[11], and *PCM1*[43] (Fig. S14A and Supplementary Data 7D). This is in line with prior studies on long neuronal genes with complex isoform structures that span multiple regulatory domains [44,45].

Together, these results demonstrate that SCZ-associated dysregulation in midbrain dopaminergic neurons is shaped by 3D genome architecture (Supplementary Data 7G). In particular, downregulation within TADs and isoform-level discordance in multi-TAD genes represent key axes linking chromatin topology to SCZ genetic risk.

Discussion

Here we present the cell-type specific genomics resource from the ventral midbrain of SCZ, BD and control subjects, with 97 deeply sequenced transcriptome RNA-seq and 34 3D genome Hi-C datasets. Our dataset will provide the field with a unique resource for the in-depth interrogation of the dopamine neuron-specific transcriptome and 3D genome, featuring over 1.561 billion and 1.86 billion cis-chromosomal contacts assigned to FANS-sorted Nurr1+NeuN+ dopamine neuron and non-neuronal fractions, respectively. Furthermore, our datasets on control brains provide an important complement to other reference sets in the field, such as those that profiled human midbrain transcriptomes with single-nucleus resolution at the expense of much shallower profiling with typically <2000 expressed genes called per cell type, or 1–2 orders of magnitude below the depth accomplished here.

Our analyses reveal that SCZ-associated transcriptional dysregulation is specific to dopa neurons, with 954 differentially expressed genes enriched for pathways of neuronal connectivity and signaling. Notably, downregulated but not upregulated genes are strongly associated with SCZ heritability, in line with long-standing models of synaptic dysfunction in SCZ[46,47]. Among these, repression of dopamine transporter (*SLC6A3*) and vesicular monoamine transporter (*SLC18A2*) is in line with related findings on midbrain RNA isolates from an independent schizophrenia cohort[13]. Furthermore, transcript-level analyses uncovered genes with both concordant and discordant transcript regulation, with discordant exhibiting greater structural complexity, spanning multiple TADs, and including high-penetrance SCZ loci such as *NRXN1*, *FOXP1*, *MAPK10*, and *PCM1*.

Importantly, we also identify a striking region- and cell-type-specific divergence: while midbrain dopa neurons show downregulation linked to genetic risk, cortical regions (DLPFC and ACC) show risk enrichment among upregulated genes, although single-nucleus studies have instead reported stronger enrichment among downregulated genes[48]. This apparent anti-correlation suggests that risk-associated pathways are engaged across multiple nodes of the dopaminergic circuitry, but the directionality of regulation depends on brain region and cell type. We acknowledge that the comparison involves different data modalities (sorted midbrain neurons versus cortical homogenates), and therefore should be interpreted cautiously. Nonetheless, the observed bidirectional changes raise the possibility of circuit-level imbalances in SCZ pathophysiology, a hypothesis that could be more directly tested in future studies incorporating cell-type-specific cortical data.

The integration of transcriptomic dysregulation with midbrain Hi-C maps further demonstrates that downregulated genes within TADs are preferentially enriched for SCZ risk variants, consistent with 3D genome organization constraining disease-relevant regulation. Gene with discordant Tx regulation, in particular, was most strongly enriched within TADs and often mapped to genes spanning multiple domains, highlighting the contribution of complex chromosomal architectures to SCZ vulnerability.

Taken together, our study provides the most comprehensive resource to date for dopaminergic neuron-specific transcriptomic and 3D genomic landscapes in SCZ. Beyond establishing midbrain dopaminergic repression as a key axis of disease risk, our findings underscore the importance of integrating multi-omic and multi-regional data to capture the distributed and circuit-dependent nature of transcriptional dysregulation in SCZ. Future studies linking cortical and subcortical regulatory landscapes across development and disease will be essential to pinpoint chromosomal "hotspots" of complex regulation that underlie SCZ pathophysiology.

Methods

All brain specimens were obtained with informed consent and/or through brain donation programs from the NIMH Human Brain Collection Core (HBCC). NIMH HBCC specimens were collected under NIH Institutional Review Board protocols 90-M-0142 and 17-M-0173 until 2018, after which HBCC research was determined to be nonhuman subjects research, with oversight by the HBCC Oversight Committee. All procedures followed institutional guidelines from the Institutional Review Boards of the brain banks for the use of postmortem human brain tissue.

RNA-Seq library preparation and nuclei isolation

An aliquot of tissue was dissected from each brain sample from the substantia nigra (A10) area of the ventral midbrain, and dounced around 50× in 1 ml of lysis buffer (0.32 M sucrose, 5 mM $CaCl_2$, 3 mM $Mg(Ace)_2$, 0.1 mM EDTA, 10 mM Tris pH8, 0.5 mM DTT, 0.1% Triton X-100) with 400U Recombinant RNase Inhibitor (Cat. 2313; Takara Bio USA, San Jose, CA). An additional 4 ml of lysis buffer (without RNase inhibitor) was then added, and the sample solution was dounced an additional 20x until completely homogenous. The sample homogenate in lysis buffer was transferred to an ultracentrifuge tube (Polypropylene Centrifuge Tubes ⅝ x 3 ¾ in., ref. 361707; Beckman Coulter, Indianapolis, IN) and underlayed with 9 ml of sucrose buffer (1.8 M sucrose, 3 mM $Mg(Ace)_2$, 0.5 mM DTT, 10 mM Tris-HCl pH8),

which was then ultracentrifuged in a SureSpin 630 (17 mL) Rotor (Cat. 79363; Thermo Fisher Scientific, Asheville, NC) with 24,000 rpm (106,803 x *g*) for 1 h at 4 °C. After removing the supernatant post-centrifugation, the nuclei pellet was resuspended in 1 ml of 0.1% BSA and transferred to a sterile 1.5 ml tube. 2 μl of Anti-Nurr1 antibody (Anti-Nurr1 antibody produced in rabbit, Cat. N4663 or Anti-NR4A2 (N-terminal) antibody produced in rabbit, Cat. N6413, lot no. 118K0446V; Sigma-Aldrich, St. Louis, MO) conjugated in a 2:1 ratio to secondary antibody Alexa Fluor 647 (Goat anti-Rabbit IgG (H + L) Highly Cross-Adsorbed Secondary Antibody, Alexa Fluor™ 647, Cat. A21245, lot no. 2098544; Invitrogen, Waltham, MA) and 1.5 μl of NeuN neuronal antibody pre-conjugated to Alexa Fluor 488 (Anti-NeuN Antibody, clone A60, Alexa Fluor™ 488 conjugated, Cat. MAB377X, lot nos. 3481408, 3193849, and 3072355; MilliporeSigma, Burlington, MA) were then added to the sample, and the sample was incubated on a rotator at 4 °C for 2 h while protected from light. After 2 h, 1 μl of nucleophilic dye DAPI (4',6-Diamidino-2-Phenylindole, Dihydrochloride, Cat. D1306; Invitrogen, Molecular Probes, Eugene, OR) was added to the sample. A BD FACSAria Cell Sorter (BD Life Sciences, San Jose, CA) was used to sort approximately 50,000 nuclei each of NeuN+/Nurr1+ and NeuN-/Nurr1- nuclei populations into collection tubes pre-filled with Trizol LS Reagent (Cat. 10296028; Invitrogen, Life Technologies, Carlsbad, CA). In our hands, 50,000 nuclei as input material was optimal for generating high-quality RNA-seq libraries with the method and procedures described here. The remaining types of nuclei were not sorted and discarded. After sorting, the sorted sample volume was measured and compared to the volume of Trizol LS Reagent pre-filled in the tube, and if necessary, additional Trizol LS was added to bring the sample to a 3:1 volume ratio of Trizol LS to sample. Sorted samples in Trizol LS were then vortexed, flash-frozen, and stored at −80 °C (Fig. S1A, B).

NeuN/Nurr1 double-positive and double-negative samples were removed from −80 °C and thawed on ice in an RNase-free environment. An additional 20% volume of Trizol LS was added to each sample, then the samples were vortexed for 30 s and incubated at room temperature for 10 min. As per the Trizol LS Reagent User Guide (Pub. No. MAN0000806; Invitrogen, Life Technologies, Carlsbad, CA), chloroform was added to each sample at 0.2 ml chloroform per 0.75 ml of total Trizol LS, and the samples were vortexed and incubated at room temperature for 3 min. Samples were then centrifuged for 15 min at 12,000 × *g* at 4 °C, after which the aqueous phase containing RNA was transferred to a sterile 1.5 ml tube. Next, the RNA samples were purified using the Zymo RNA Clean & Concentrator™ −5 kit (Cat. R1014; Zymo Research, Irvine, CA), including an in-column DNase I treatment, which was incubated for 30 min instead of the recommended 15 min. During the final step of that kit, RNA was eluted into 8.5 μl of nuclease-free water. Lastly, the ArcticZymes Heat & Run gDNA Removal Kit (Cat. 80200; ArcticZymes Technologies, Tromsø, Norway) was used as a secondary DNase treatment to remove genomic DNA from each sample.

Library preparation and sequencing

Before performing the ArcticZymes DNase treatment, the RNA concentration and RNA integrity number (RIN) were obtained for each sample using the Agilent RNA 6000 Pico kit (Cat. 5067-1513; Agilent, Santa Clara, CA) on the Agilent 2100 Bioanalyzer system. Those values were used to determine the sample input into the SMARTer® Stranded Total RNA-Seq Kit v2 - Pico Input Mammalian (Cat. 634413; Takara Bio USA, San Jose, CA), which was used to generate cDNA libraries for sequencing. The complete libraries were sequenced by the New York Genome Center on the Illumina NovaSeq-6000 platform, with 100 bp paired-end reads at a depth of approximately 60 million read pairs per sample. We have assembled a dataset comprising 111 RNA-seq libraries, originating from FANS-sorted Nurr1 + /NeuN+ immuno-tagged midbrain dopaminergic neurons, as well as their neighboring glial and other non-neuronal nuclei (Nurr1-/NeuN-) (Fig. S1A, B). These 111 RNA-seq libraries are categorized into 53 samples of dopaminergic neurons and 58 samples of non-neuronal cells. Within the dopaminergic neuron subset, 28 are designated as control samples, 14 are from subjects diagnosed with schizophrenia, and 11 are from subjects diagnosed with BD. Among the non-neuronal samples, 28 represent controls, 22 are from subjects diagnosed with SCZ, and 8 are from subjects diagnosed with BD (Fig. 1A and Supplementary Data 1).

RNA-seq data processing, alignment, and quality control

For the analysis of RNA sequencing data, the initial steps involved the alignment and pre-processing of raw reads. *Trimmomatic (v0.36)*[49] was employed to trim the raw reads, followed by the mapping of the processed reads to the human reference genome GRCh38.v24[50] using *STAR (v2.5.3a)*[51] (Fig. S2A). The resulting BAM files contained paired-end reads that were successfully mapped, inclusive of those spanning splice junctions. After alignment, expression quantification was performed and summarized at both the gene and transcript levels using GENCODE v27 annotations[52,53]. Quality control measures, including checks for sample mislabeling, genotype discrepancies, and sex mislabeling, were conducted on 97 RNAseq libraries using the `mbv` function from *QTLtools (v1.3)*[54] (Fig. S2B–E). A scatterplot of $\log_2$(CPM) expression for the XIST (chrX) and UTY (chrY) genes confirmed accurate annotation of reported biological sex for all donors (Fig. S2F).

Deconvolution of dopa neuron and non-neuronal samples

To estimate dopaminergic and non-neuronal cell-type proportions per sample for both dopa and non-neuronal fractions, we applied the MuSiC[21] tool using a reference single-cell RNA-seq dataset from Wang et al.[22] of the human midbrain. Top 50 DEGs per annotated cluster were used as reference cell type-specific markers. The reference comprised all 11 clusters, annotated as microglia (1), astrocytes (2), oligodendrocytes (0, 3), endothelial cells (4), oligodendrocyte progenitor cells (5), neurons (6, 7, 9), fibroblast-like cells (10), pericytes (8), and T cells (11). For downstream modeling, we grouped clusters into three categories: dopa neurons (clusters 6, 7), non-dopa neurons (cluster 9), and non-neuronal populations (all other clusters) (see Fig. 1C and S2E). Deconvolution was performed using the `music_prop` function with cluster identities and sample metadata derived from the reference Seurat object.

Data normalization, selection of covariates, and statistical analysis of differences in gene expression of cases and controls

Raw gene expression counts were normalized using the `voomWithDreamWeights` function[55]. Filtering was applied to retain only expressed genes, defined as those with counts-per-million (CPM) values greater than 5 in at least 10% of the samples. This step was done separately on three datasets: (1) Dopa and non-neuronal (2) Dopa neuronal, and (3) non-neuronal samples

Covariates were identified across the above mentioned three datasets through forward stepwise model selection using the `mvForwardStepwise` function from the *mvIC* R package *(V1.6.3)* [56], employing the Bayesian Information Criterion (BIC) for model comparison. Specifically, each additional covariate was tested to ensure the BIC difference between models was at least 5. After this, our final models for all comparisons are following:

1) Dopa vs. non-neurons in controls:
   Dopa and Non-neurons expression: ~celltype + RIN + (1| Sex) + Age + Age^2 + PMI + GC content
2) SCZ vs. controls and BD vs. controls comparisons in dopa neuronal samples:
   Dopa neurons expression: ~Diagnosis + RIN + (1 | Sex) + Age + Age^2 + PMI + (1 | adapters) + GC content + dopa proportion (cluster 7)
3) SCZ vs. controls and BD vs. controls comparisons in non-neuronal samples:

Non-neurons expression: ~Diagnosis + RIN + (1 | Sex) + Age + Age^2 + PMI + GC content + Non-neuron proportion (cluster 0)

Briefly, celltype in (1) is a categorical variable defined as dopa or non-neuronal, RIN is RNA Integrity Number, which is a measure of RNA quality, and Dx is the Diagnosis (SCZ, BD, and Controls). Figure 2A, S2.BA, and S3A illustrate the variance explained by identified covariates in gene expression for three datasets utilizing the variancePartition[55,57]. Statistical analysis to measure the significant gene expression changes across all comparisons was performed using the *dream* function from the variancePartition[55,57].

To assess potential confounding by antipsychotic exposure (e.g., Haldol, chlorpromazine), we performed a secondary differential expression analysis restricted to SCZ cases. Toxicology data were used to classify individuals as antipsychotic-exposed or -unexposed. Our models were following

1) Antipsychotic exposed vs. unexposed in dopaminergic neurons from SCZ/BD:

   Dopa neurons expression: ~Antipsychotic status + RIN + (1 | Sex) + scale(age) + scale(age^2) + scale(PMI) + (1 | adapters) + GC_NC_20_39 + dopa proportions (cluster 7)

2) Antipsychotic exposed vs. unexposed in non-neurons from SCZ/BD:

Non-neurons expression: ~Antipsychotic status + RIN + (1 | Sex) + scale(age) + scale(age^2) + scale(PMI) + GC_NC_20_39 + Non-neuron proportions (cluster 0)

remaCorr analysis of differences in Tx expression

To reduce the impact of multiple testing in transcript-level analyses, we utilized omnibus testing frameworks grounded in meta-analysis. Specifically, we implemented fixed-effects (FE) meta-analysis for correlated test statistics. To capture transcript-level dysregulation beyond overall gene expression changes, we used the R-based tool remaCorr (Random Effects Regression for Transcript-Level Expression)[58]; specifically the `mvTest()` function. remaCorr applies a fixed-effects meta-analytic model to aggregate transcript-level effect sizes (log2FC for SCZ vs. controls or BD vs. controls in this study) for each gene, and tests whether at least one transcript deviates from the overall gene-level pattern. Crucially, remaCorr does not test transcripts individually. Instead, it generates a single *p*-value per gene, reflecting whether there is significant heterogeneity in transcript usage between groups. This design enables detection of relative isoform abundance changes, even when total gene expression remains stable, capturing regulatory events such as isoform switching, alternative promoter usage, or splicing differences. A similar methodological framework has been applied in Kosoy et al.[29,30].

Input to remaCorr, we used the transcript-level *fit* object derived from the *voom* transformation and linear modeling using the `limma` framework with the DREAM method from the `variancePartition` package, which accounts for complex random effects.

The remaCorr test was run using the following command:

```
variancePartition::mvTest(fit = fit_Tx, vobj = vobjDream_Tx, features = gene_features, coef = "DxSCZ - DxControl", method = "remaCorr")
```

HiC library preparation and sequencing; Hi-C comprehensively detects genome-wide chromatin interactions in the cell nucleus. Considering the intricate packaging of 2 m of DNA within a nucleus with a diameter of 2 μm, the nucleus is compartmentalized into territories occupied by single chromosomes. Zooming into these territories reveals two compartments: active A-compartments and inactive B-compartments. These compartments consist of numerous interaction clusters known as TADs, distributed throughout the nucleus, where chromatin of the same compartment type is associated. Additionally, loops, which are specific points of interaction between distant chromatin regions, further contribute to the three-dimensional organization of the genome.

Hi-C nuclei isolation and fixation

An aliquot of tissue was dissected from each brain sample from the substantia nigra (A10) area of the ventral midbrain, and dounced 50–70× in 5 ml of lysis buffer (0.32 M sucrose, 5 mM $CaCl_2$, 3 mM $Mg(Ace)_2$, 0.1 mM EDTA, 10 mM Tris pH8, 0.5 mM DTT, 0.1% Triton X-100) until completely homogenous. The sample was transferred to a 15 ml conical tube, and 5 ml of sucrose buffer (1.8 M sucrose, 3 mM $Mg(Ace)_2$, 0.5 mM DTT, 10 mM Tris-HCl, pH 8) was added. The sample was inverted and mixed to incorporate the sucrose, then centrifuged for 10 min at 2300 × *g* at 4 °C. After removing the supernatant, the sample pellet was resuspended in 4 ml of lysis buffer, formaldehyde was added to a final concentration of 1%, and the sample was incubated on a rotator for 5 min at room temperature. After that, glycine was added to a final concentration of 217 mM, and the sample was again incubated on a rotator for 5 min at room temperature. Next, the sample was centrifuged for 5 min at 2300 × *g* at 4 °C, and the supernatant was removed. The sample was then resuspended in 5 ml of lysis buffer, and transferred to an ultracentrifuge tube (Polypropylene Centrifuge Tubes ⅝ x 3 ¾ in., ref. 361707; Beckman Coulter, Indianapolis, IN), underlayed with 9 ml of sucrose buffer (1.8 M sucrose, 3 mM $Mg(Ace)_2$, 0.5 mM DTT, 10 mM Tris-HCl pH8), and ultracentrifuged in a SureSpin 630 (17 mL) Rotor (Cat. 79363; Thermo Fisher Scientific, Asheville, NC) with 24,000 rpm (106,803 × *g*) for 1 h at 4 °C. After removing the supernatant post-centrifugation, the nuclei pellet was resuspended in 1 ml of 0.1% BSA, passed through a 40 μm cell strainer, and transferred to a sterile 1.5 ml tube. Two microliters of Anti-Nurr1 antibody (Anti-Nurr1 antibody produced in rabbit, Cat. N4663 or Anti-NR4A2 (N-terminal) antibody produced in rabbit, Cat. N6413; Sigma-Aldrich, St. Louis, MO) conjugated in a 2:1 ratio to secondary antibody Alexa Fluor 647 (Goat anti-Rabbit IgG (H + L) Highly Cross-Adsorbed Secondary Antibody, Alexa Fluor™ 647, Cat. A21245; Invitrogen, Waltham, MA) and 1.5 μl of NeuN neuronal antibody pre-conjugated to Alexa Fluor 488 (Anti-NeuN Antibody, clone A60, Alexa Fluor™ 488 conjugated, Cat. MAB377X; MilliporeSigma, Burlington, MA) were then added to the sample, and the sample was incubated on a rotator at 4 °C for 2h while protected from light. After 2h, 1 μl of nucleophilic dye DAPI (4′,6-Diamidino-2-Phenylindole, Dihydrochloride, Cat. D1306; Invitrogen, Molecular Probes, Inc., Eugene, OR) was added to the sample. A BD FACSAria Cell Sorter (BD Life Sciences, San Jose, CA) was used to sort approximately 6000 nuclei each of NeuN+/Nurr1+ and 50,000 NeuN-/Nurr1- nuclei populations into collection tubes coated with 5% BSA and pre-filled with 300 μl of DPBS. After sorting, samples were centrifuged for 5 min at 2300 × *g* at 4 °C. The supernatant was removed, and the pellet was stored at −80 °C. In our hands, 5000–50,000 nuclei were ideal as input for high-quality Hi-C libraries with the protocol listed below.

Arima Hi-C library prep and sequencing

Post-FANS sorting, approximately 6000 dopaminergic neuronal nuclei (NeuN+/Nurr1+) and 50,000 sorted glia (NeuN−/Nurr1−) were processed through the Hi-C method using the Arima-HiC Kit User Guide for Mammalian Cell Lines (Cat. A510008; Arima Genomics, San Diego, CA). Subsequently, they were purified using the Beckman Coulter SPRIselect Beads (Cat. B23318; Indianapolis, IN). Then, the samples were sonicated utilizing the Covaris S220 (Woburn, MA), targeting 300–500 base pairs fragment sizes, then size selected and purified using Beckman Coulter SPRIselect Beads to a target of 300–500 base pairs. The samples were then biotin-enriched using the Arima-HiC Kit for Library Preparation, alongside the Swift Biosciences® Accel-NGS® 2S Plus DNA Library Kit (Cat. A101020; Arima Genomics, San Diego, CA). Afterward, the Swift Biosciences Accel-NGS 2S Plus DNA library kit

(Cat. 21024; Ann Arbor, MI) was utilized for end repair and adapter ligation. Unique indices were ligated to each sample from the Swift Biosciences 2S Indexing Kit (Cat. 26148; Ann Arbor, MI). DNA libraries were amplified and purified using the Kapa Hyper Prep Kit (Cat. NC0709851; Kapa Biosystems, Wilmington, MA) and Beckman Coulter AMPure® SPRIselect Beads. Final libraries were sequenced through Illumina NovaSeq 6000 technology at the New York Genome Center at 150 bp paired-end sequencing, at 400 million reads per sample.

HiC data processing

We have assembled a dataset comprising 34 HiC libraries, originating from FANS-sorted Nurr1+/NeuN+ immuno-tagged midbrain dopaminergic neurons, as well as their neighboring glial nuclei (Nurr1−/NeuN−). These 34 HiC libraries are categorized into 17 samples of dopa neurons and 17 samples of non-neuronal cells (Fig. 1A and Supplementary Data 6).

Alignment and preprocessing

In our exploration of the spatial organization of differentially regulated genes, we utilized the *HiCpro* (*v3.1.0*) pipeline[59]. We performed alignment using the UCSC's hg38 genome and generated non-duplicated valid interaction pairs, and we recorded the genomic interactions reported by ligated reads. The quality of analysis results in each step was evaluated, including inter-/intra-chromosomal pairs, chimeric pairs, duplicates, intra-fragment, intra-long distance ranges, and ligations. The interaction matrices were generated at different bin sizes, like 20 kb, 40 kb, 150 kb, 500 kb, and 1 mb. We used HicRep (*v1.12.2*)[36], QTLtools (*v1.3*)[60], and PCA for quality check, outlier detection and to find mislabeled samples (Figure. S11).

Following the initial processing steps, we transitioned to the transformation of HiCpro output into a more suitable format for downstream analysis. Utilizing the hicprojuicebox tool (a hicpro utils), we converted the HiCpro output into.hic format, which was then further processed into.cool format using hicConvertFormat (*v2.2.1.1*)[61]. This allowed for seamless integration with the HiCExplorer toolkit, where we proceeded to normalize interactions using hicNormalize and apply correction methods with hicCorrectMatrix (v2.2.1.1)[61], including the Knight–Ruiz balancing algorithm with default parameters. These steps were essential for preparing the data for subsequent analyses of chromatin organization and gene regulation in dopaminergic neurons. For identifying TADs, we utilized TopDom[37], while compartment calling was performed using CscoreTools (v*1.1*). Additionally, loop calling was conducted using HICCUPS (*juicer_tools_1.22.01*)[37,39,62].

Loop discovery

Chromatin loops were detected using the juicer tool HICCUPS at resolutions of 5, 10, and 25 kb, employing default window sizes. Only loops that were reproducible across two resolutions were kept and advanced to the next step of analysis. It's important to note that our analysis specifically targeted chromatin loops within chromosomes, disregarding interchromosomal interactions to focus solely on intra-chromosomal interactions.

Compartment discovery

To identify chromatin compartments, we used CscoreTool[39], which performs eigenvector decomposition of normalized Hi-C contact matrices to assign compartment scores (PC1 values). Positive PC1 values indicate active (A) compartments, while negative values represent inactive (B) compartments. Because eigenvector-based compartment scores can arbitrarily flip sign between chromosomes or runs, we implemented a sign-alignment step based on transcriptional activity. For each chromosome, we calculated the mean expression of genes overlapping positive and negative compartments (CPM > 0.5 in ≥10% of samples). If the negative-score regions showed higher mean expression, we inverted the sign of that chromosome's compartment scores, ensuring that positive values consistently represent transcriptionally A compartments and negative values represent B compartments. This correction was applied separately to dopaminergic and non-neuronal datasets.

Valid interaction pairs were generated using HiC-Pro, and compartment scores were computed separately for each cell type at multiple resolutions (10, 30, 50, 60, 70, 80, and 100 kb). For all downstream analyses, we used the 50 kb resolution matrices, which provided an optimal balance between resolution and signal robustness. Each genomic bin was assigned to compartment A or B based on the (sign-aligned) PC1 score, and the absolute value of the score was retained to represent compartment strength. To assess cell-type-specific compartment switching, we compared compartment calls between Dopa and non-neuronal cells and classified bins into four categories: (1) A in both cell types, (2) B in both cell types, (3) A in Dopa and B in Non-neurons, (4) B in Dopa and A in Non-neurons.

TAD discovery

For TAD identification, we implemented a custom R-based workflow built around TopDom v0.0.2[37]. First, .cool format HiC matrices were converted to full chromosome-wise contact matrices at 10, 50, and 100 kb resolution using the HiCcompare v1.20.0 (ref. 63) and cooler2bedpe[64] tools. For each chromosome (chr1–22), contact matrices from all samples were summed bin-by-bin to generate deep coverage consensus matrices for each cell type. We then ran TopDom separately on these merged matrices using a window size of 60, 70, 80, 90, 100, 110, 120, 130, 140, 150, 160, 170, 180, and 200 (optimized empirically), identifying domain boundaries based on local minima in contact frequency ("binSignals") Our analysis revealed that a contact matrices at 10 kb with window size of 50 provided the best results (Fig. S13A, B). This process resulted in 5966 TADs in dopaminergic neurons and 6348 TADs in non-neuronal cells.

Disease trait enrichment analysis using MAGMA

We utilized MAGMA (*v1.08b*)[23] to perform trait enrichment analysis for both brain-related and non-brain-related traits. The gene lists used for this analysis were derived from limma and remaCorr analyses, as described in the previous sections. Our goal was to assess the enrichment of these GWAS traits in cell-region- and disease-specific genes. MAGMA calculates gene-level *p*-values for each gene and trait by jointly analyzing the association of all SNPs from GWAS summary statistics that map to the gene region, while accounting for linkage disequilibrium (LD) between SNPs. Gene regions were defined as 35 kb upstream and 10 kb downstream of the gene body. LD was estimated using data from the European panel of the 1000 Genomes Project phase 3[65]. Finally, using a linear regression framework, MAGMA tested whether differentially expressed genes showed stronger associations with GWAS traits compared to the rest of the genome.

Functional pathway analysis

Functional pathway analysis was done using gene set enrichment analysis (GSEA)[66], specifically using the fisher's exact test as the method for the test. The gene lists used for this analysis were derived from limma and remaCorr analyses, as described in the previous sections. The resulting gene set enrichment analysis identifies key biological processes, pathways, or functional gene groups in which the input differentially expressed genes are significantly enriched.

Reporting summary

Further information on research design is available in the Nature Portfolio Reporting Summary linked to this article.

Data availability

All raw sequencing data generated in this study, including Hi-C and RNA-seq FASTQ files, have been deposited in the NCBI Gene

Expression Omnibus (GEO) under accession number GSE311978 and GSE311979 for RNAseq and HiC data respectively. Source data are provided with this paper.

Code availability

All analyses in the manuscript were conducted using existing, publicly available tools, including variancePartition for mixed-model expression analysis, remaCorr for transcript-level aggregation, and TopDom for TAD calling. Because we relied entirely on established and openly available packages, no additional custom code was necessary. All the required code is made available at https://codeocean.com/capsule/2247653/tree.

References

1. Espeso-Gil, S. et al. A chromosomal connectome for psychiatric and metabolic risk variants in adult dopaminergic neurons. *Genome Med.* **12**, 19 (2020).
2. Singh, T. et al. Rare coding variants in ten genes confer substantial risk for schizophrenia. *Nature* **604**, 509–516 (2022).
3. Gandal, M. J. et al. Shared molecular neuropathology across major psychiatric disorders parallels polygenic overlap. *Focus* **17**, 66–72 (2019).
4. Skene, N. G. et al. Genetic identification of brain cell types underlying schizophrenia. *Nat. Genet.* **50**, 825–833 (2018).
5. Girdhar, K. et al. The neuronal chromatin landscape in adult schizophrenia brains is linked to early fetal development. *medRxiv* https://doi.org/10.1101/2023.10.02.23296067 (2023).
6. Girdhar, K. et al. Chromatin domain alterations linked to 3D genome organization in a large cohort of schizophrenia and bipolar disorder brains. *Nat. Neurosci.* **25**, 474–483 (2022).
7. Hannon, E. et al. DNA methylation meta-analysis reveals cellular alterations in psychosis and markers of treatment-resistant schizophrenia. *Elife* **10**, e58430 (2021).
8. Benjamin, K. J. M. et al. Sex affects transcriptional associations with schizophrenia across the dorsolateral prefrontal cortex, hippocampus, and caudate nucleus. *Nat. Commun.* **15**, 3980 (2024).
9. Benjamin, K. J. M. et al. Analysis of the caudate nucleus transcriptome in individuals with schizophrenia highlights effects of antipsychotics and new risk genes. *Nat. Neurosci.* **25**, 1559–1568 (2022).
10. Kohen, R., Dobra, A., Tracy, J. H. & Haugen, E. Transcriptome profiling of human hippocampus dentate gyrus granule cells in mental illness. *Transl. Psychiatry* **4**, e366 (2014).
11. Lanz, T. A. et al. Postmortem transcriptional profiling reveals widespread increase in inflammation in schizophrenia: a comparison of prefrontal cortex, striatum, and hippocampus among matched tetrads of controls with subjects diagnosed with schizophrenia, bipolar or major depressive disorder. *Transl. Psychiatry* **9**, 151 (2019).
12. Howes, O. D. & Kapur, S. The dopamine hypothesis of schizophrenia: version III-the final common pathway. *Schizophr. Bull.* **35**, 549–562 (2009).
13. Purves-Tyson, T. D. et al. Putative presynaptic dopamine dysregulation in schizophrenia is supported by molecular evidence from post-mortem human midbrain. *Transl. Psychiatry* **7**, e1003 (2017).
14. Muench, J. & Hamer, A. M. Adverse effects of antipsychotic medications. *Am. Fam. Physician* **81**, 617–622 (2010).
15. Wei, J. et al. Single nucleus transcriptomics of ventral midbrain identifies glial activation associated with chronic opioid use disorder. *Nat. Commun.* **14**, 5610 (2023).
16. Agarwal, D. et al. A single-cell atlas of the human substantia nigra reveals cell-specific pathways associated with neurological disorders. *Nat. Commun.* **11**, 4183 (2020).
17. Smajić, S. et al. Single-cell sequencing of human midbrain reveals glial activation and a Parkinson-specific neuronal state. *Brain* **145**, 964–978 (2022).
18. Hoffman, G. E. et al. Commonmind consortium provides transcriptomic and epigenomic data for schizophrenia and bipolar disorder. *Sci. Data* **6**, 180 (2019).
19. Zetterström, R. H. et al. Dopamine neuron agenesis in Nurr1-deficient mice. *Science* **276**, 248–250 (1997).
20. Jacobs, F. M. J. et al. Identification of Dlk1, Ptpru and Klhl1 as novel Nurr1 target genes in meso-diencephalic dopamine neurons. *Development* **136**, 2363–2373 (2009).
21. Wang, X., Park, J., Susztak, K., Zhang, N. R. & Li, M. Bulk tissue cell type deconvolution with multi-subject single-cell expression reference. *Nat. Commun.* **10**, 380 (2019).
22. Wang, Q. et al. Molecular profiling of human substantia nigra identifies diverse neuron types associated with vulnerability in Parkinson's disease. *Sci. Adv.* **10**, eadi8287 (2024).
23. de Leeuw, C. A., Mooij, J. M., Heskes, T. & Posthuma, D. MAGMA: generalized gene-set analysis of GWAS data. *PLoS Comput. Biol.* **11**, e1004219 (2015).
24. Kogure, M. et al. Association of SLC6A3 variants with treatment-resistant schizophrenia: a genetic association study of dopamine-related genes in schizophrenia. *Front. Psychiatry* **14**, 1334335 (2023).
25. Huang, S.-Y. et al. Association of promoter variants of human dopamine transporter gene with schizophrenia in Han Chinese. *Schizophr. Res.* **116**, 68–74 (2010).
26. Gandal, M. J. et al. Transcriptome-wide isoform-level dysregulation in ASD, schizophrenia, and bipolar disorder. *Science* **362**, eaat8127 (2018).
27. Collado-Torres, L. et al. Regional heterogeneity in gene expression, regulation, and coherence in the frontal cortex and hippocampus across development and schizophrenia. *Neuron* **103**, 203–216.e8 (2019).
28. Wen, C. et al. Cross-ancestry atlas of gene, isoform, and splicing regulation in the developing human brain. *Science* **384**, eadh0829 (2024).
29. Lin, D.-Y. & Sullivan, P. F. Meta-analysis of genome-wide association studies with overlapping subjects. *Am. J. Hum. Genet.* **85**, 862–872 (2009).
30. Kosoy, R. et al. Alzheimer's disease transcriptional landscape in ex vivo human microglia. *Nat. Neurosci.* 1830–1843. https://doi.org/10.1038/s41593-025-02020-2 (2025).
31. Han, B. et al. A general framework for meta-analyzing dependent studies with overlapping subjects in association mapping. *Hum. Mol. Genet.* **25**, 1857–1866 (2016).
32. Waheed, Z. et al. The role of Tau proteoforms in health and disease. *Mol. Neurobiol.* **60**, 5155–5166 (2023).
33. Irimia, M. et al. A highly conserved program of neuronal microexons is misregulated in autistic brains. *Cell* **159**, 1511–1523 (2014).
34. Hervoso, J. L. et al. Splicing-specific transcriptome-wide association uncovers genetic mechanisms for schizophrenia. *Am. J. Hum. Genet.* **111**, 1573–1587 (2024).
35. Kośla, K. et al. The WWOX gene influences cellular pathways in the neuronal differentiation of human neural progenitor cells. *Front. Cell. Neurosci.* **13**, 391 (2019).
36. Lin, D., Sanders, J. & Noble, W. S. HiCRep.py: fast comparison of Hi-C contact matrices in Python. *Bioinformatics* **37**, 2996–2997 (2021).
37. Shin, H. et al. TopDom: an efficient and deterministic method for identifying topological domains in genomes. *Nucleic Acids Res.* **44**, e70 (2016).
38. Dong, P. et al. Population-level variation in enhancer expression identifies disease mechanisms in the human brain. *Nat. Genet.* **54**, 1493–1503 (2022).
39. Zheng, X. & Zheng, Y. CscoreTool: fast Hi-C compartment analysis at high resolution. *Bioinformatics* **34**, 1568–1570 (2018).
40. Sebastian, R. et al. Schizophrenia-associated NRXN1 deletions induce developmental-timing- and cell-type-specific vulnerabilities in human brain organoids. *Nat. Commun.* **14**, 3770 (2023).

41. Kirov, G. et al. Neurexin 1 (NRXN1) deletions in schizophrenia. *Schizophr. Bull.* **35**, 851–854 (2009).
42. Ingason, A. et al. Expression analysis in a rat psychosis model identifies novel candidate genes validated in a large case-control sample of schizophrenia. *Transl. Psychiatry* **5**, e656 (2015).
43. Gurling, H. M. D. et al. Genetic association and brain morphology studies and the chromosome 8p22 pericentriolar material 1 (PCM1) gene in susceptibility to schizophrenia. *Arch. Gen. Psychiatry* **63**, 844–854 (2006).
44. Zufferey, M., Tavernari, D., Oricchio, E. & Ciriello, G. Comparison of computational methods for the identification of topologically associating domains. *Genome Biol.* **19**, 217 (2018).
45. Javierre, B. M. et al. Lineage-specific genome architecture links enhancers and non-coding disease variants to target gene promoters. *Cell* **167**, 1369–1384.e19 (2016).
46. Howes, O. D. & Shatalina, E. Integrating the neurodevelopmental and dopamine hypotheses of schizophrenia and the role of cortical excitation-inhibition balance. *Biol. Psychiatry* **92**, 501–513 (2022).
47. Exposito-Alonso, D. & Rico, B. Mechanisms underlying circuit dysfunction in neurodevelopmental disorders. *Annu. Rev. Genet.* **56**, 391–422 (2022).
48. Ruzicka, W. B. et al. Single-cell multi-cohort dissection of the schizophrenia transcriptome. *Science* **384**, eadg5136 (2024).
49. Bolger, A. M., Lohse, M. & Usadel, B. Trimmomatic: a flexible trimmer for Illumina sequence data. *Bioinformatics* **30**, 2114–2120 (2014).
50. Frankish, A. et al. GENCODE reference annotation for the human and mouse genomes. *Nucleic Acids Res.* **47**, D766–D773 (2019).
51. Dobin, A. et al. STAR: ultrafast universal RNA-seq aligner. *Bioinformatics* **29**, 15–21 (2013).
52. Harrow, J. et al. GENCODE: the reference human genome annotation for The ENCODE Project. *Genome Res.* **22**, 1760–1774 (2012).
53. The GENCODE Consortium.GENCODE - Human Release 27 GRCh38.p10) (2017). Available at https://www.gencodegenes.org/human/release_27.html.
54. Fort, A. et al. MBV: a method to solve sample mislabeling and detect technical bias in large combined genotype and sequencing assay datasets. *Bioinformatics* **33**, 1895–1897 (2017).
55. Hoffman, G. E. & Schadt, E. E. variancePartition: interpreting drivers of variation in complex gene expression studies. *BMC Bioinform.* **17**, 483 (2016).
56. Hoffman G. mvIC: Multivariate Information Criteria to identify important predictors in high dimensional multivariate regression. R package version 1.6.3, https://github.com/GabrielHoffman/mvIC (2022).
57. Robinson, M. D., McCarthy, D. J. & Smyth, G. K. edgeR: a bioconductor package for differential expression analysis of digital gene expression data. *Bioinformatics* **26**, 139–140 (2010).
58. Hoffman, G. Random effects meta-analysis for correlated test statistics [R package remaCor version 0.0.20]. *Comprehensive R Archive Network (CRAN)* https://CRAN.R-project.org/package=remaCor (2025).
59. Servant, N. et al. HiC-Pro: an optimized and flexible pipeline for Hi-C data processing. *Genome Biol.* **16**, 259 (2015).
60. Delaneau, O. et al. A complete tool set for molecular QTL discovery and analysis. *Nat. Commun.* **8**, 15452 (2017).
61. Wolff, J. et al. Galaxy HiCExplorer 3: a web server for reproducible Hi-C, capture Hi-C and single-cell Hi-C data analysis, quality control and visualization. *Nucleic Acids Res.* **48**, W177–W184 (2020).
62. Durand, N. C. et al. Juicer provides a one-click system for analyzing loop-resolution Hi-C experiments. *Cell Syst.* **3**, 95–98 (2016).
63. Stansfield, J. C., Cresswell, K. G., Vladimirov, V. I. & Dozmorov, M. G. HiCcompare: an R-package for joint normalization and comparison of HI-C datasets. *BMC Bioinform.* **19**, 279 (2018).
64. Abdennur, N. & Mirny, L. A. Cooler: scalable storage for Hi-C data and other genomically labeled arrays. *Bioinformatics* **36**, 311–316 (2020).
65. 1000 Genomes Project Consortium et al. A global reference for human genetic variation. *Nature* **526**, 68–74 (2015).
66. Subramanian, A. et al. Gene set enrichment analysis: a knowledge-based approach for interpreting genome-wide expression profiles. *Proc. Natl. Acad. Sci. USA* **102**, 15545–15550 (2005).

Acknowledgements

We thank the patients and families who donated material for these studies. Brain tissue for the study was obtained through the Human Brain Collection Core (HBCC) brain bank. We thank the computational resources and staff expertise provided by the Scientific Computing at the Icahn School of Medicine at Mount Sinai. We sincerely thank the members of the Roussos Lab and the Akbarian Lab for their valuable help with data analysis and for engaging in insightful discussions. This work was supported, in part, through the computational resources and staff expertise provided by Scientific Computing at the Icahn School of Medicine at Mount Sinai. We are extremely grateful to J. Ochando and other personnel of the Icahn School of Medicine at Mount Sinai's Flow Cytometry Core for providing and teaching cell-sorting expertise. Funding: This project was supported by NIH U01DA048279 and R01DA047880 (S.A. and P.R.) and NIMH-IRP project # ZIC MH002903 for the HBCC. This research was supported [in part] by the Intramural Research Program of the National Institutes of Health (NIH). The contributions of the NIH author(s) were made as part of their official duties as NIH federal employees, are in compliance with agency policy requirements, and are considered Works of the United States Government. However, the findings and conclusions presented in this paper are those of the author(s) and do not necessarily reflect the views of the NIH or the U.S. Department of Health and Human Services.

Author contributions

S.S. and K.G. contributed to the conceptualization, formal analysis, investigation, and methodology of the study. They were responsible for project administration, resources, validation, and visualization. J.B. and G.E.H. developed and supervised the RNA-seq analysis pipeline and contributed to validation. B.Z. and M.W. provided single-cell R data objects for deconvolution analysis. M.I., T.L., A.V., N.S., and V.E. contributed to data generation and data curation. S.M. and P.K.A. provided resources, including postmortem tissue. K.G., P.R., and S.A. contributed to study design, investigation, resources, and supervision.

Competing interests

The authors declare no competing interests.

Additional information

Supplementary information The online version contains supplementary material available at https://doi.org/10.1038/s41467-026-71281-7.

Correspondence and requests for materials should be addressed to Kiran Girdhar, Panos Roussos or Schahram Akbarian.

Peer review information *Nature Communications* thanks Jennifer Erwin and the other anonymous reviewer(s) for their contribution to the peer review of this work. A peer review file is available.